IEEE Access
Multidisciplinary | Rapid Review | Open Access Journal

Received August 14, 2017, accepted September 12, 2017, date of publication September 18, 2017,
date of current version October 12, 2017.

Digital Object Identifier 10.1109/ACCESS.2017.2753796

Underwater Image Restoration via Maximum Attenuation Identification

NAN WANG, (Member, IEEE), HAIYONG ZHENG, (Member, IEEE), AND BING ZHENG, (Member, IEEE)

Department of Electronic Engineering, College of Information Science and Engineering, Ocean University of China, Qingdao 266100, China

Corresponding author: Haiyong Zheng (zhenghaiyong@ouc.edu.cn)

This work was supported in part by the National Natural Science Foundation of China under Grant 61703381, in part by the Natural Science Foundation of Shandong Province under Grant ZR2017BF006, in part by the China Postdoctoral Science Foundation under Grant 2016M590658, and in part by Fundamental Research Funds for the Central Universities under Grant 201713017.

ABSTRACT Underwater images are difficult to process because of low contrast and color distortion. The in-water light propagation model was proposed several years ago but is relatively complicated to be used in reality. In this paper, the full underwater light propagation model is simplified to be used as the transmission model. On the basis of this model, we propose a new method, called maximum attenuation identification, to derive the depth map from degraded underwater images. At the same time, regional background estimation is implemented to ensure optimal performance. Experiments on three groups of images, namely, natural underwater scene, calibration board, and colormap board, are conducted. We report the quantitative and qualitative comparisons of our approach with existing state-of-the-art approaches. The performance evaluation on contrast enhancement and color restoration validates that our approach outperforms existing state-of-the-art approaches.

INDEX TERMS Image processing, underwater technology, image restoration, image enhancement.

I. INTRODUCTION

The underwater world contains abundant resources. Thus, the corresponding exploration has significance in the commercial and scientific research areas. Although sonar is still the primary technique used to detect underwater signal in the long range, the photoelectric sensor technique plays an irreplaceable role in the aspect of close observation and object detection because it can provide high time and space resolution and intuitive visual information. However, images captured underwater always present a low quality because of the special propagation characteristic of light in water [1], which is mainly depicted as absorption and scattering [2], [3]. Researchers have employed several methods, such as laser line scanning [4], laser range gate [5], and optical polarization imaging [6], [7], to obtain high-quality images. Although these methods can improve the imaging quality, the corresponding imaging systems, particularly the physical apparatus, are costly. As a low-cost but effective method, digital image processing is still the primary approach used to improve the quality of images captured by underwater optical cameras [2], [8].

Two methods, namely, image restoration and image enhancement, are employed to improve underwater image quality [2], [8]. Image restoration aims to recover the degraded image based on the physical degradation model and the information about the degraded image. The most commonly used restoration method is reverse convolution, which is based on the degradation model and expressed as

$$g(x, y) = h(x, y) * f(x, y) + \eta(x, y) \tag{1}$$

where $g(x, y)$ and $f(x, y)$ denote the degraded and original images, respectively; $h(x, y)$ is the degradation function; $\eta(x, y)$ is the noise model. The key issues of this method are how to construct the degradation model (or specifically, the point spread function [PSF]) correctly and obtain the parameters accurately. Aside from the classical Jaffe-McGlamery model [9], several restoration algorithms have been proposed. Hou *et al.* [10] incorporated the underwater optical properties into the traditional image restoration approach, measured the in-water optical properties, and used these properties in deriving the PSF and modulation transfer function (MTF). Trucco and Olmos [11] presented a self-tuning restoration filter based on a simplified version of the Jaffe-McGlamery image formation model. Liu *et al.* [12] determined the PSF and MTF of seawater in the laboratory by means of image transmission theory and used Wiener filters

to restore the blurred underwater images. Wang *et al.* [13] used layering estimation to obtain a precise degradation model. Lu *et al.* [14] proposed a high-turbidity underwater image super-resolution algorithm by descattering and fusion. Although the results of model-based restoration methods are rigorous, a fatal drawback of model-based restoration is that it requires many parameters, which are scarcely known in reality and can be relatively variable.

Image enhancement does not rely on the physical characteristic and model. The main algorithms include histogram modification, homomorphic filtering, multiwave denoising, edge enhancement, and color balancing. Classical algorithms, such as CLAHE [15] and Retinex [16], have been proven effective through experiments. On the basis of these enhancement methods, researchers have proposed several integrated underwater image enhancement algorithms [17]–[22]. Although such algorithms can provide visually pleasing results sometimes, they may also induce color distortion and noise amplification, particularly in turbid water. Establishing a general and effective underwater image enhancement method is still a necessary and challenging work.

II. RELATED WORK AND MAIN PROBLEMS IN UNDERWATER IMAGE PROCESSING

The intricacies presented by the underwater environment are far more than that presented by the terrestrial environment. However, with some simplification, the underwater environment is similar to haze weather. From this aspect, underwater image enhancement may be transformed into a dehazing problem. Compared with underwater image processing, image dehazing has been well investigated [23]. Recently, several researchers have applied deep neural networks to dehaze underwater images and obtained interesting results [24], [25]. Specifically, the illumination-scattering model is widely used to remove haze [26]–[28]. With some prior knowledge, the transmission map is first estimated and the restored image can then be obtained. Among the types of prior knowledge, the dark channel prior (DCP) algorithm [29] may be the most popular and has been conducted in underwater image processing [30], [31]. At the same time, several variants based on DCP, such as red channel [32] and GB channel [33], are proposed. Such algorithms consider the special underwater propagating situation, but all use the dark channel as the principal step (which is conducted by identifying the lowest intensity pixel in a local patch).

However, after thousands of underwater images are observed, we determine that prior knowledge supporting the effectiveness of DCP is inappropriate for underwater images. The two main reasons for the difference are as follows: First, the type of objective image is not the same. Thus, DCP assumes that the image shows nearly the entire object and that part of the background (e.g., sky area) is not the major part. However, in the water environment, objects in one natural captured image always exist sparsely. Moreover, the background area (i.e., the infinite distance part) will appear in every part of the image, surrounding the objects. Second, DCP considers that fog will lead to a high intensity of the dark channel of the image, which indicates that the local intensity will increase with the dense depth. However, this phenomenon is completely reversed underwater. Moreover, the infinite distance may result in infinite black in the ocean. Thus, on the basis of the two points, we believe that prior knowledge should be reconsidered to obtain good image restoration performance during underwater image processing. Furthermore, the two main aspects of underwater image degradation are low contrast and color distortion. If we do not compensate for the attenuation of different light wavelengths, then color distortion cannot be solved.

In this study, we propose a maximum attenuation identification (MAI)-based method to dehaze and correct the color distortion of underwater images. The attenuation effect, which consists of absorption and scattering, is assumed to be strongly correlated with imaging depth. Thus, we first derive the depth map according to the attenuation situation. The illumination-scattering model is changed to formulate the attenuation formation as a simplification of the underwater light model. We apply the proposed method to three groups of underwater images to test its performance subjectively and objectively. The remainder of the paper is organized as follows: Section III describes the underwater imaging model and its transformation. Section IV discusses the MAI-based underwater image restoration method in detail. Section V presents the experimental results. Section VI provides the conclusion.

III. UNDERWATER LIGHT MODEL

The full underwater model described by Duntley [1] is generally expressed as

$$\begin{aligned} {}_tN_r(z,\theta,\phi) = {}& {}_tN_0(z_t,\theta,\phi)e^{(-\alpha(z)r)} \\ & + N(z_t,\theta,\phi)e^{(K(z,\theta,\phi)rcos\theta)} \\ & \times(1-e^{(-\alpha(z)r+K(z,\theta,\phi)rcos\theta)}). \end{aligned} \quad (2)$$

where ${}_tN_r(z,\theta,\phi)$ is the observed radiance, which is a function of the depth of the observer z; θ and ϕ are the zenith and azimuth angles between the observer and the target, respectively. The observed radiance is a mixture of the radiance at the subject, ${}_tN_0(z_t,\theta,\phi)$, and the radiance in the water column (i.e., the airlight), $N(z_t,\theta,\phi)$. In these terms, z_t represents the depth of the target. The attenuation coefficient $\alpha(z)$ is the sum of two terms, namely, the scattering and absorption coefficients. The distance between the observer and the target is denoted by r. The radiance attenuation function, $K(z,\theta,\phi)$, indicates how the airlight changes with depth. If we assume that the water is homogeneous, then the effect of K is seldom appreciable. Thus, the full underwater model 2 can be simplified as

$${}_tN_r(z,\theta,\phi) =_t N_0(z_t,\theta,\phi)e^{(-\alpha r)} + N(z_t,\theta,\phi)(1-e^{(-\alpha r)}). \quad (3)$$

Notably, the attenuation coefficient α in model 3 is the sum of the scattering and absorption coefficients, that is, $\alpha = \alpha_s + \alpha_a$. The absorption effect is the most different part between foggy ambient and in-water situations, which cannot be ignored underwater. Moreover, according to the measurement and statistical data, light with different wavelengths involves different in-water absorption parameters. Fig. 1 shows that the absorption coefficient of red light ($600 \sim 700\ nm$) is higher than that of green and blue light. Thus, the R, G, and B color channels should be considered separately underwater.

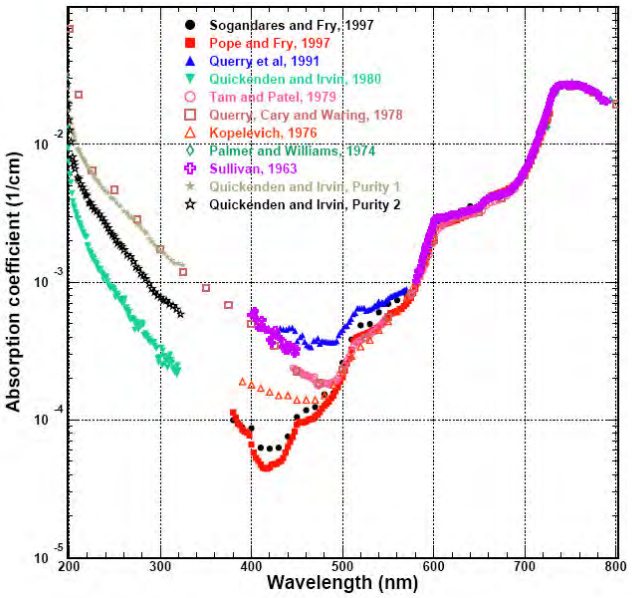

FIGURE 1. Statistical data of the absorption coefficients for different wavelengths.

Another important factor that should be considered is the illumination situation. In the atmosphere, the background tends to be bright because of sunlight. However, in the water, the infinite background light is black because of absorption. Fig. 2 shows a group of raw images captured in different types of ocean water and the corresponding dark channel images. According to DCP, the dark channel of a hazy image will present a high intensity in regions with dense haze. However, the real situation of underwater images (e.g., the images shown in Fig. 2) is that the dark channel of a distant area tends to be zero, whereas that of a near object, which is bright, exhibits a high intensity. The difference between atmospheric and underwater situations is caused by the absorption aspect. Thus, according to light absorption, computing the dark channel of underwater images makes little sense.

Another simple underwater prior knowledge is that the light intensity will decay as an exponential function of distance. The irradiance E at position r can be modeled as

$$E(r) = E(0)e^{(-\alpha r)} \tag{4}$$

where α is the total attenuation coefficient of the medium. Thus, we can rewrite model 3 in the imaging end as

$$I(\mathbf{x}) = J(\mathbf{x})\xi(\mathbf{x}) + A(1 - \xi(\mathbf{x})) \tag{5}$$

where I is the observed intensity, which corresponds to ${}_tN_r(z, \theta, \phi)$; J is the object radiance; A is the global background light; $\xi = e^{(-\alpha r)}$ is the medium transmission coefficient; $\mathbf{x}$ is the vector of the coordinates. In such manner, the entire underwater model is similar to the popular illumination-scattering model, which is usually used as dehazing model and can be described as

$$I(\mathbf{x}) = J(\mathbf{x})t(\mathbf{x}) + A(1 - t(\mathbf{x})) \tag{6}$$

The only difference between models 5 and 6 is that ξ consists of the absorption and scattering effects, whereas t always describes only the scattering part in dehazing situation.

IV. MAI-BASED METHOD

A. ESTIMATING THE BACKGROUND LIGHT

Accurate background light estimation is the basis of a good restoration effect. We assume that the background part lies in the most distant part of the picture. Thus, the most fundamental job is deriving the depth map.

According to Eq. 4, the farther from the camera, the lower the intensity. Moreover, further analyses show that the absorption of different wavelengths differs. The red color travels a shorter distance than do the blue and green colors. At the same time, according to Rayleigh scattering theory, the shorter wavelengths of green and blue light will scatter more than the longer wavelength of red light [31]. Comprehensively considering the two factors, we can deduce that, with a long distance, the total power of the red color will be lower than those of the blue and green colors, which can be expressed as

$$\begin{aligned} E^R(r) &< E^G(r) \\ E^R(r) &< E^B(r) \end{aligned} \tag{7}$$

where E is the irradiance, which is the same meaning as that in Eq. 4; R, G, and B represent red, green, and blue, respectively. Thus, the red color can be used to derive the depth map because it is most sensitive to the change in distance.

First, we filter the red color with a maximum filter of a window size that can be modulated to derive the depth map of the image. Then, we select the top 10% lowest pixels. Corresponding to these pixels, the pixels in the original image I are selected as the background. Subsequently, background light estimation is conducted on the basis of these pixels. Furthermore, in the atmosphere, the background light can be considered uniform. However, illumination is always nonuniform underwater. Thus, assuming that the entire background is the same may be inappropriate. Moreover, the background of an underwater image is always surrounding the object. Thus, the background should be estimated in a highly detailed manner. In this study, we slice the input image into $n \times n$ pieces to identify the background. Similar to the effect of

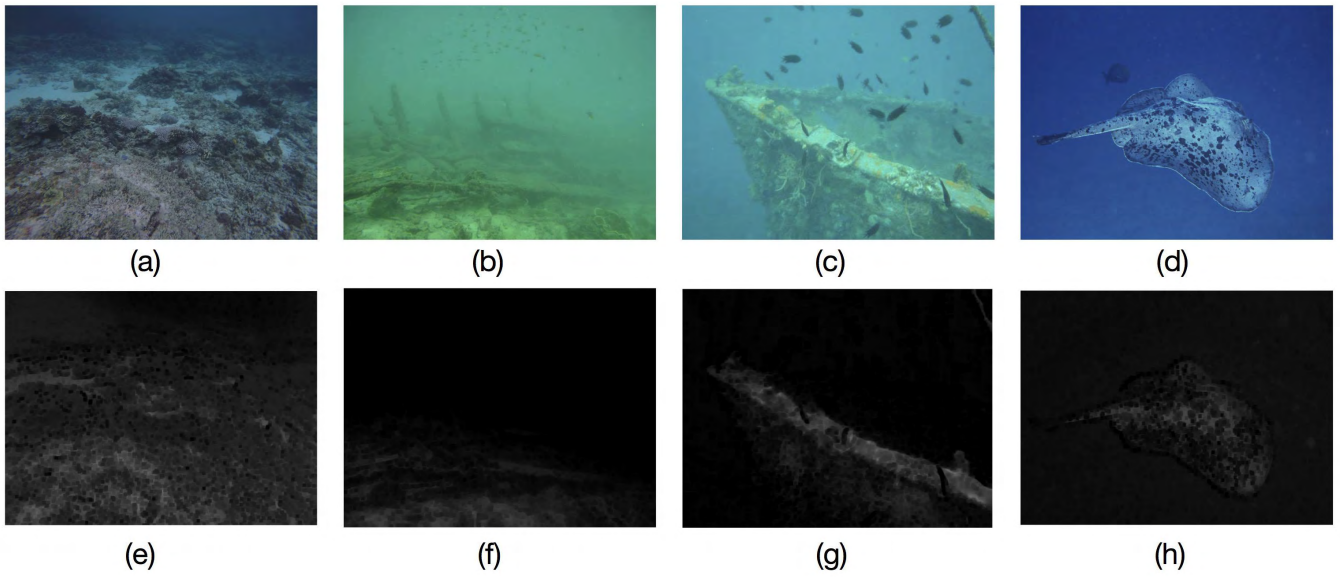

FIGURE 2. (a-d) Original images captured in different types of ocean water and (e-h) the corresponding dark channel images.

patch size, the larger the value of n, the rougher the estimation background, and vice versa. At the same time, n should not be small because a small n exhibits a low possibility of background existing in the window. We recommend that n be equal to 2 or 3.

Figs. 3 and 4 show the most haze-opaque regions and the corresponding background light estimation for MAI and DCP, respectively. Obviously, the regions detected as the background area by our MAI method are accurate. By contrast, the DCP method incorrectly detects regions with high intensity as the background areas. Notably, the background pixels detected by our MAI method are far from the small dark objects in the original images (e.g., the small fish in Figs. 3(b) and 3(c)). At the same time, compared with the estimation background images shown in Figs. 3 and 4, the colors of our estimation background are more similar to the original background of the raw images, making MAI a good foundation for color correction.

B. ESTIMATING THE TRANSMISSION

Assuming that the transmission and background light in a local patch $\Omega(x)$ is constant, we calculate the maximum intensity in the local patch on both sides of Eq. 5. As analyzed previously, the attenuation α for different colors with different wavelengths is relatively distinct because of the different attenuation and scattering coefficients. Thus, the attenuation α must be considered particularly for colors R, G, and B. Hence, we rewrite model 5 as

$$\begin{aligned}
\max_{\mathbf{y}\in\Omega(\mathbf{x})}(I^R(\mathbf{y})) &= \xi(\mathbf{x})\max_{\mathbf{y}\in\Omega(\mathbf{x})}(J^R(\mathbf{y})) + A(\mathbf{x})^R(1-\xi^R(\mathbf{x})) \\
\max_{\mathbf{y}\in\Omega(\mathbf{x})}(I^G(\mathbf{y})) &= \xi(\mathbf{x})\max_{\mathbf{y}\in\Omega(\mathbf{x})}(J^G(\mathbf{y})) + A(\mathbf{x})^G(1-\xi^G(\mathbf{x})) \\
\max_{\mathbf{y}\in\Omega(\mathbf{x})}(I^B(\mathbf{y})) &= \xi(\mathbf{x})\max_{\mathbf{y}\in\Omega(\mathbf{x})}(J^B(\mathbf{y})) + A(\mathbf{x})^B(1-\xi^B(\mathbf{x})),
\end{aligned} \tag{8}$$

where 1 denotes the normalized unity. Correspondingly, A, J and I need to be normalized to range [0,1]. Given that A and ξ can be considered constant in the patch, they can be placed outside of the max operators. Taking color R as an example, we continue to transform the function as

$$\begin{aligned}
1-\max_{\mathbf{y}\in\Omega(\mathbf{x})}(I^R(\mathbf{y})) = \xi^R(\mathbf{x})(1-\max_{\mathbf{y}\in\Omega(\mathbf{x})}(J^R(\mathbf{y}))) \\
+(1-\xi^R(\mathbf{x}))(1-A^R(\mathbf{x})).
\end{aligned} \tag{9}$$

Then, we divide $1-A^R(\mathbf{x})$ on both sides as

$$\begin{aligned}
\frac{1-\max_{\mathbf{y}\in\Omega(\mathbf{x})}(I^R(\mathbf{y}))}{1-A^R(\mathbf{x})} &= 1-\xi^R(\mathbf{x}) \\
&\quad +\xi^R(\mathbf{x})\frac{1-\max_{\mathbf{y}\in\Omega(\mathbf{x})}(J^R(\mathbf{y}))}{1-A^R(\mathbf{x})}
\end{aligned} \tag{10}$$

We further normalize the equation as

$$\begin{aligned}
(1-\frac{1-\max_{\mathbf{y}\in\Omega(\mathbf{x})}(J^R(\mathbf{y}))}{1-A^R(\mathbf{x})})\xi(\mathbf{x}) \\
= 1-\frac{1-\max_{\mathbf{y}\in\Omega(\mathbf{x})}(I^R(\mathbf{y}))}{1-A^R(\mathbf{x})}.
\end{aligned} \tag{11}$$

First, we consider the attenuation of the part near the site. Commonly, the underwater background light A is dark, particularly in the deep sea. Thus, the intensities of A in the three colors R, G, and B are always low. At the same time, with the appropriate patch window size, the maximum value of J can approximately reach unity. The lighter the object is, the more precise the assumption is. Thus, the proposed method is best performed when the object is bright. The term $\frac{1-\max_{\mathbf{y}\in\Omega(\mathbf{x})}(J^R(\mathbf{y}))}{1-A^R(\mathbf{x})}$ tends to be zero in the near field. In this

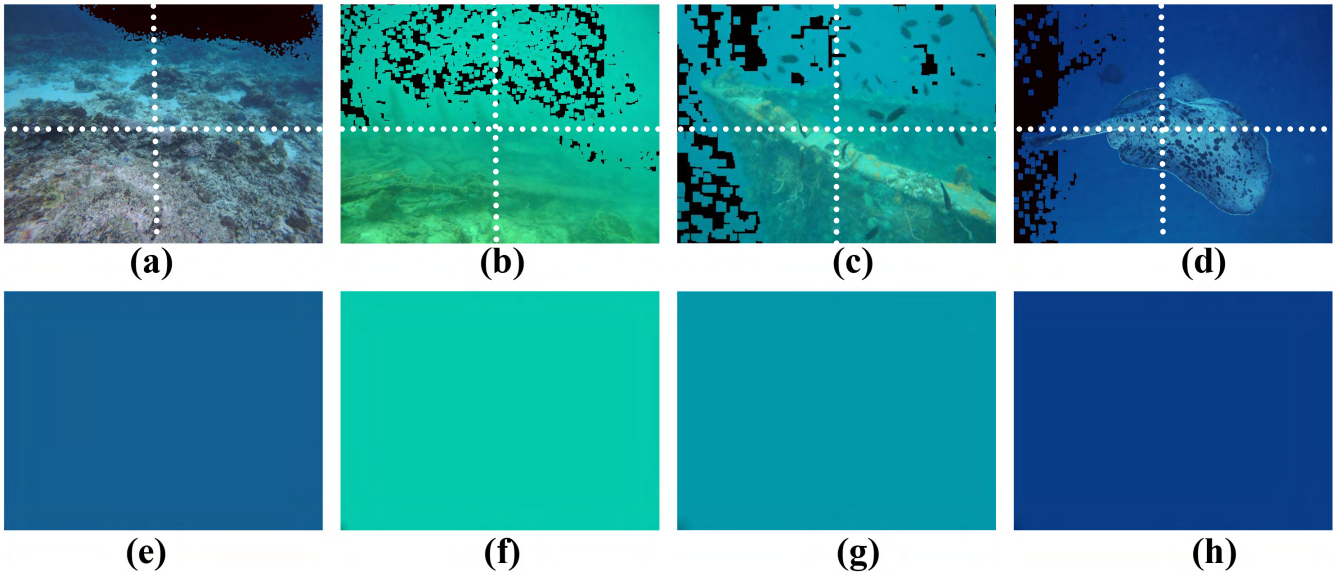

FIGURE 3. (a-d) Most haze-opaque regions detected by our MAI method shown as black (the dotted lines illustrate the sliced pieces) and (e-h) the corresponding background light estimation.

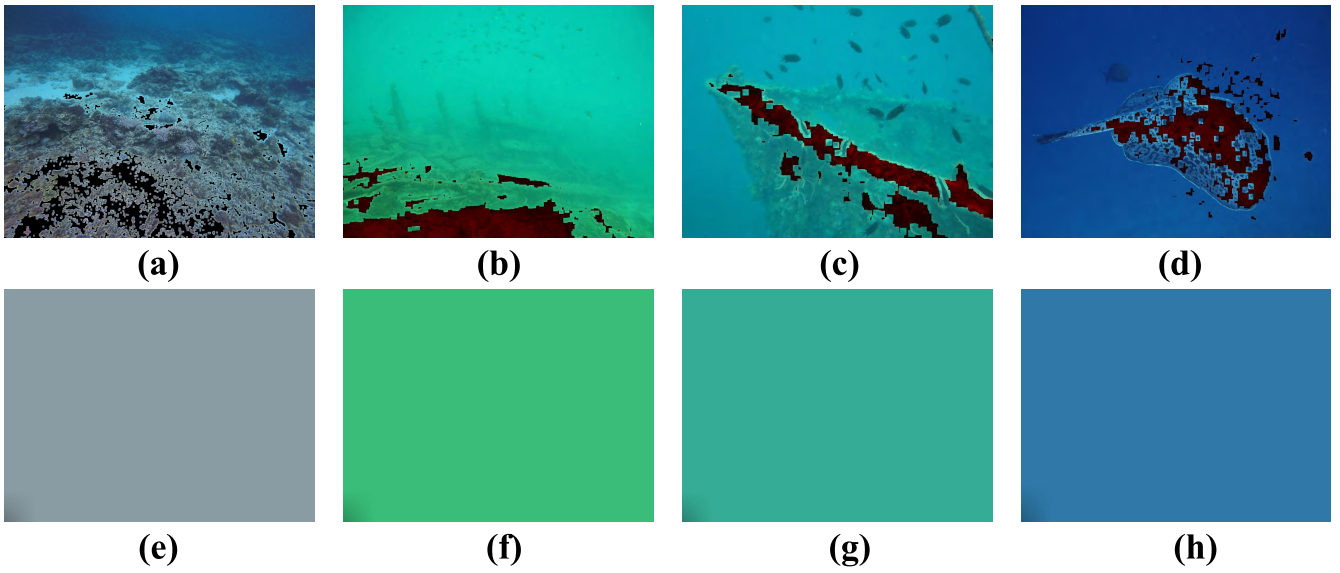

FIGURE 4. (a-d) Most haze-opaque regions detected by dark channel method shown as black and (e-h) the corresponding background light estimation.

situation, attenuation ξ can be simply estimated as

$$\xi \to 1 - \frac{1 - \max_{\mathbf{y}\in\Omega(\mathbf{x})}(I^R(\mathbf{y}))}{1 - A^R(\mathbf{x})} \tag{12}$$

According to Eq. 4, ξ tends to be 0 when $r \to \infty$ in the area with infinite distance. At the same time, Eq. 12 also yields $\xi \to 0$ at the infinite distance part of the area where the estimation background light is similar to I. Thus, Eq. 12 handles the near and far parts smoothly.

Notably, the tendency of transmission of blue and green colors is similar to that of red color. Thus, the transmission of the two colors can be computed in the same manner as that of red color. However, the intensity of the transmission of different colors differs. Therefore, the R, G, and B channels should be calculated separately.

With the estimated background light and the transmission map, we can recover the scene radiance according to Eq. 5. In practice, we need to set a limit to medium transmission ξ. On the one hand, even for the clearest water, the attenuation is smaller than unity for the absorption and scattering of water molecules. On the other hand, the transmission should be set larger than zero because a slight attenuation should be preserved to keep the restored image naturally. In our algorithm, the limit of ξ is empirically set to be $0.1 < \xi < 0.95$.

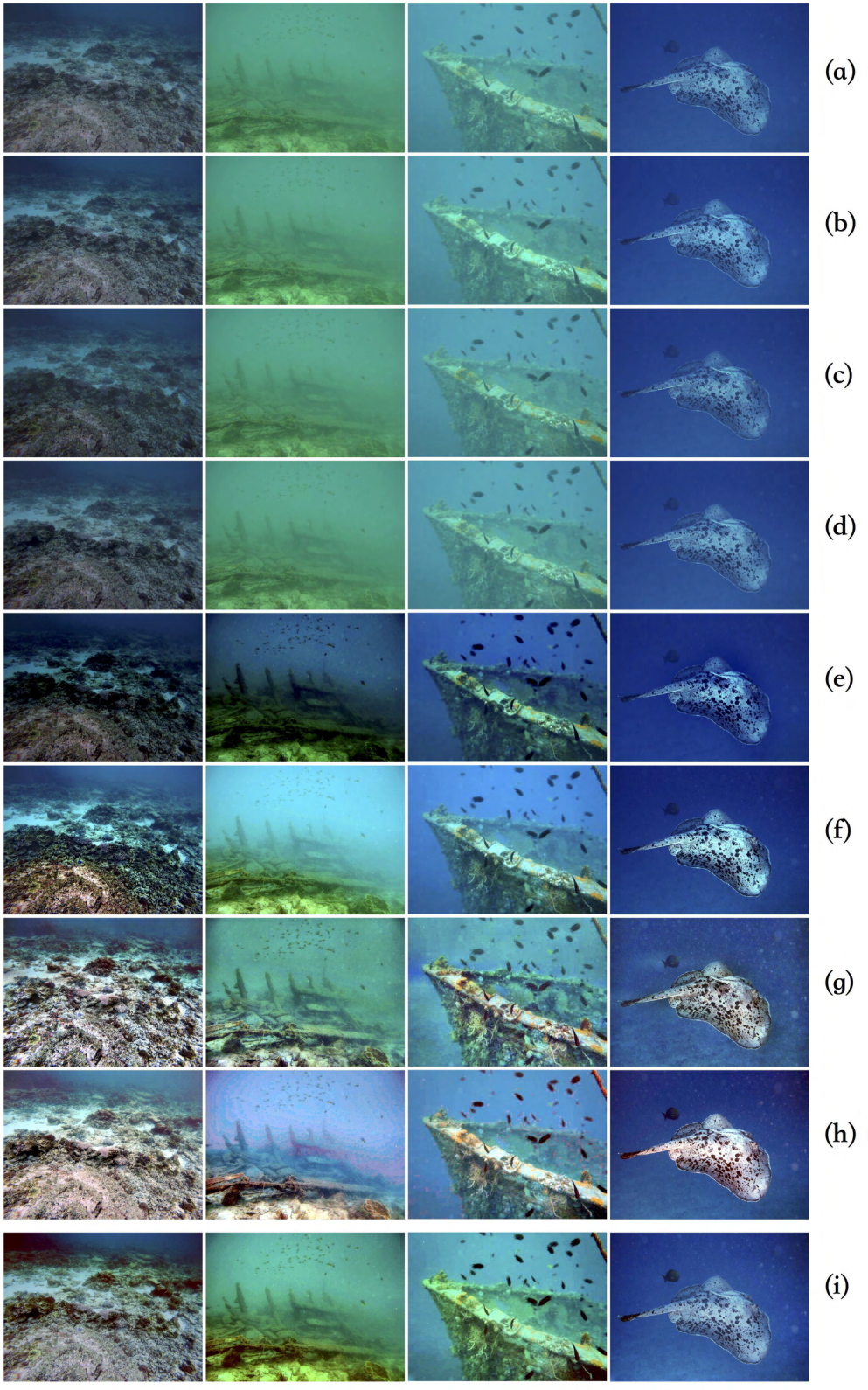

FIGURE 5. Subjective comparison of different methods on natural scene images: (a) raw images, (b) results of DCP, (c) results of CAP, (d) results of DehazeNet, (e) results of MSCNN, (f) results of NON, (g) results of CLAHE, (h) results of Retinex, and (i) results of MAI.

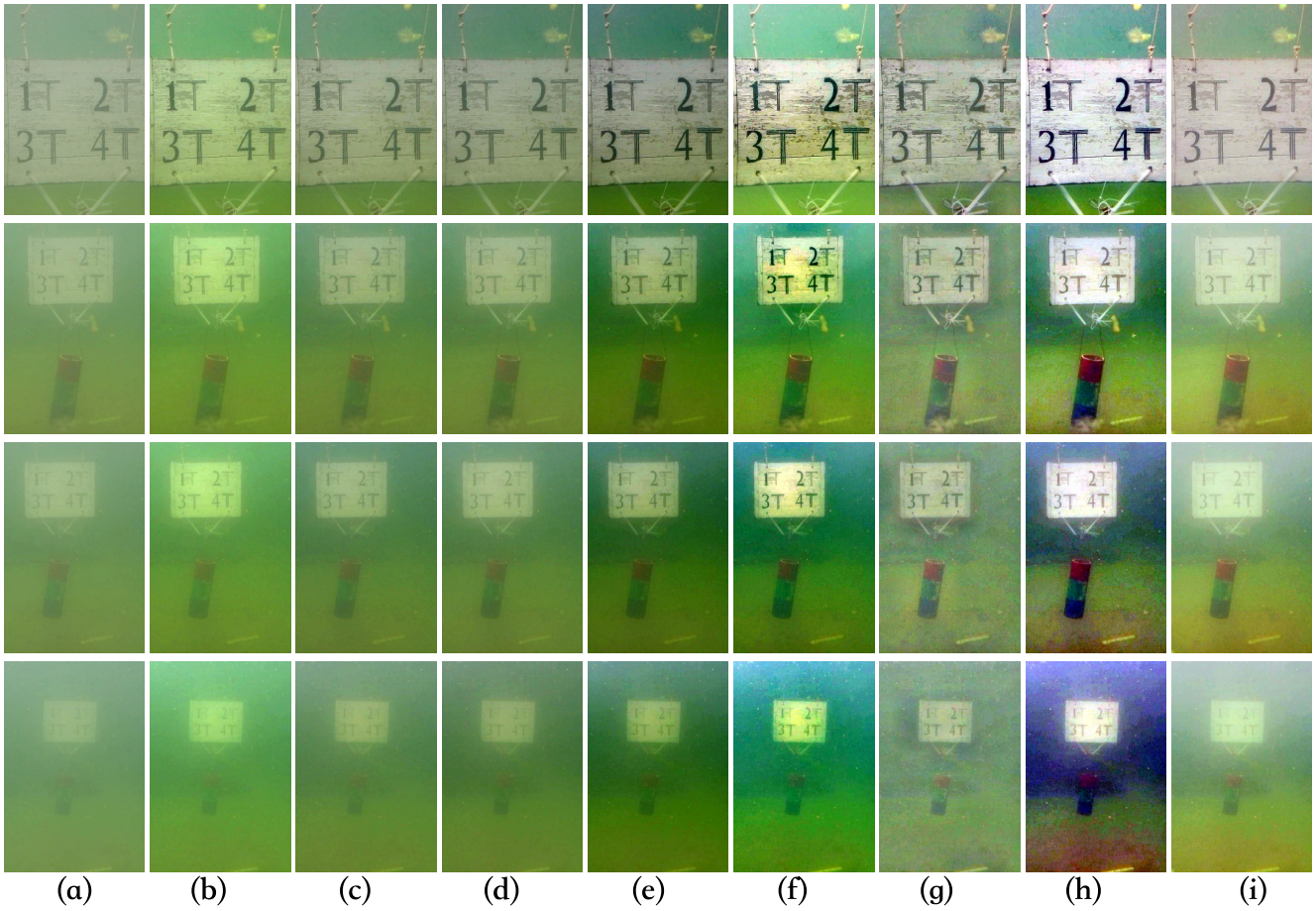

FIGURE 6. Subjective comparison of different methods on images of a calibration board coupled with a color RGB tank: (a) raw images: from top to bottom, the distances from the camera to the object are 120, 210, 270, and 360 *mm*; (b) results of DCP; (c) results of CAP; (d) results of DehazeNet; (e) results of MSCNN; (f) results of NON; (g) results of CLAHE; (h) results of Retinex; and (i) results of MAI.

V. EXPERIMENTAL RESULTS

We collect three groups of underwater images to evaluate the performance of our algorithm. The first group of images are captured by imaging of natural scenes and are widely used in underwater image processing. The two other groups are images captured under experimental situations: one is imaging of a calibration board coupled with a color RGB tank and the other is imaging of a colormap board. The distance from object to camera is changed to obtain different visibility values. We consider two classical image enhancement methods, namely, CLAHE [15] and Retinex [16]; three integrated dehazing methods, namely, DCP [29], CAP [27], and NON [23]; and two recently developed deep neural network methods, namely, DehazeNet [24] and MSCNN [25]. We also compare these methods with our proposed MAI method subjectively and objectively.

A. SUBJECTIVE PERFORMANCE EVALUATION

Fig. 5 shows the images of underwater natural scenes and the corresponding processed results. Our MAI method obtains obvious contrast enhancement and reveals a natural color scene. In the second original image, the fish group on the upper part is fuzzy. The detailed information of all the four original images is unclear because of the scattering effect. By contrast, in our processed result, the fish group is clearly visible and the detailed information, such as the black part of the tail of the fish in the last image, is clear.

Figs. 6 and 7 show the images of a calibration board coupled with a color RGB tank and a colormap board at different distances from the camera, respectively. Underwater images suffer significantly from color distortion dominated by a green tone because of the different attenuation coefficients of different wavelengths. With the increase in the distance, the color contrast and accuracy decrease. The seven counterparts (i.e., four numbers and three colors) all exhibit unbalanced contrast enhancement and color correction. For example, NON enhances the contrast most. At the same time, NON amplifies the illumination distortion and induces a bluish tone. Our algorithm performs well in color correction and contrast enhancement.

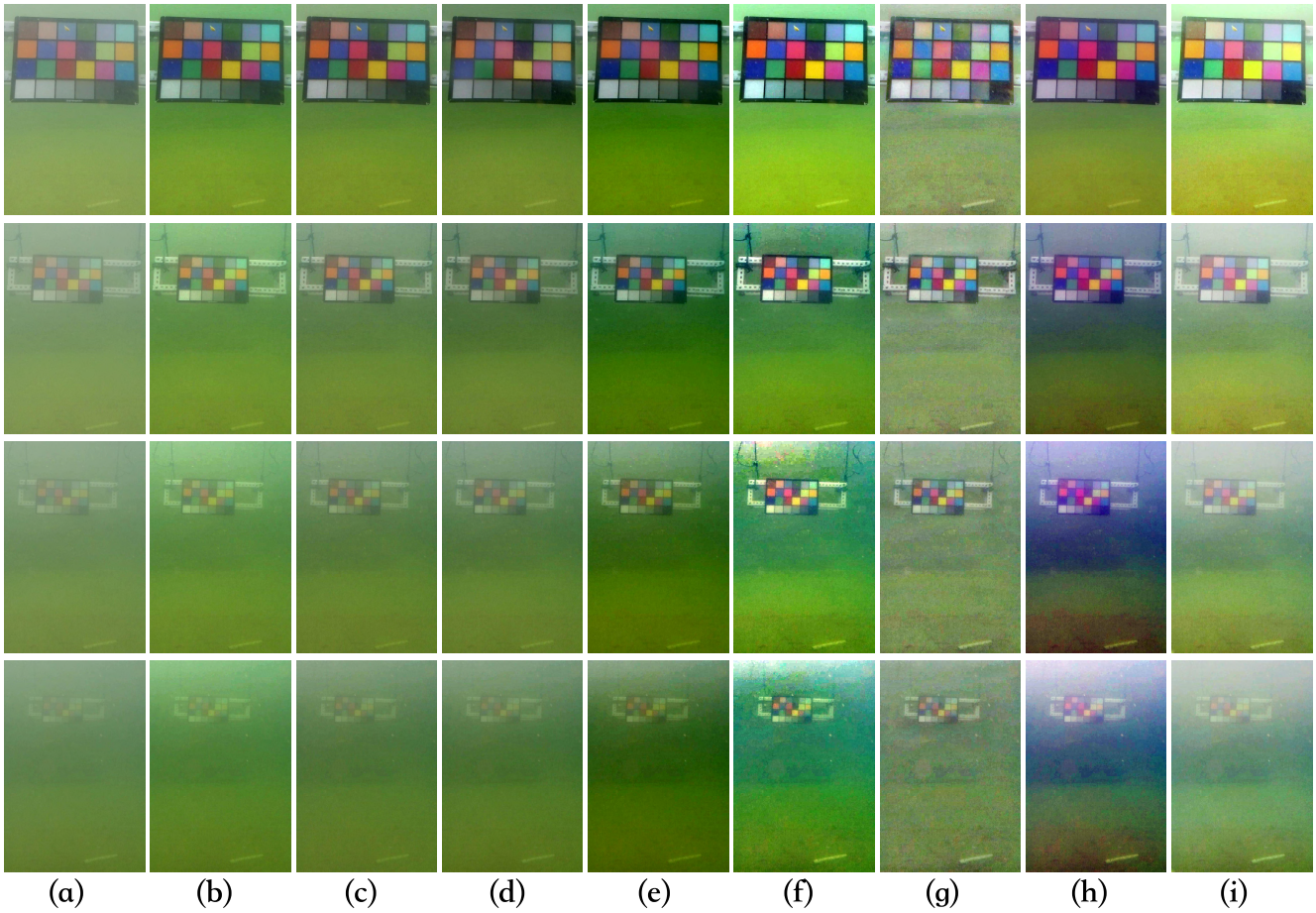

FIGURE 7. Subjective comparison of different methods on images of a colormap board: (a) raw images: from top to bottom, the distances from the camera to the object are 120, 210, 270, and 360 *mm*; (b) results of DCP; (c) results of CAP; (d) results of DehazeNet; (e) results of MSCNN; (f) results of NON; (g) results of CLAHE; (h) results of Retinex; and (i) results of MAI.

B. OBJECTIVE PERFORMANCE EVALUATION

Contrary to atmosphere images, underwater images are more difficult to restore because the corresponding reference images are hard to be acquired especially for natural underwater scenes. Thus, we use the calibration and colormap boards as the experimental objects to obtain objective results. Two major factors of an image restoration algorithm are usually considered: one is contrast enhancement together with edge restoration and the other is color correction.

1) CONTRAST AND VISIBILITY RECOVERY

In this work, we rely on a non-referenced metric proposed in [34] to evaluate the level of contrast enhancement. The assessment computes the gradient ratio at the visible edges. Three coefficients, namely, the ratio of restored edge number to original edge number (n_e), the ratio of the gradient intensity for every edge pixel (r_e), and the number of pixels that the algorithm saturates to black or white (δ), are calculated. The formulation for each coefficient is defined as

$$n_e = \frac{n_r - n_0}{n_o}, \tag{13}$$

where n_r and n_0 are the number of edges for the restored and original images, respectively. n_e evaluates the quantity of edges that are absent in the original image but present in the restored image.

$$r_e = \frac{1}{n_r} \sum_i log(r_i), \tag{14}$$

where r_i is the ratio of the gradient in the restored image to that in the original image for each pixel i. Finally, the third coefficient δ is computed as

$$\delta = \frac{n_s}{dim_x \times dim_y}, \tag{15}$$

where n_s is the number of pixels that the algorithm saturates to black or white.

As we only consider visibility recovery, we select the first two coefficients as the assessment parameters. The group of calibration board images and the corresponding processed results are taken as the assessment object. Moreover, many suspended particles in water also enter the image scope. Determining whether these particles should be considered

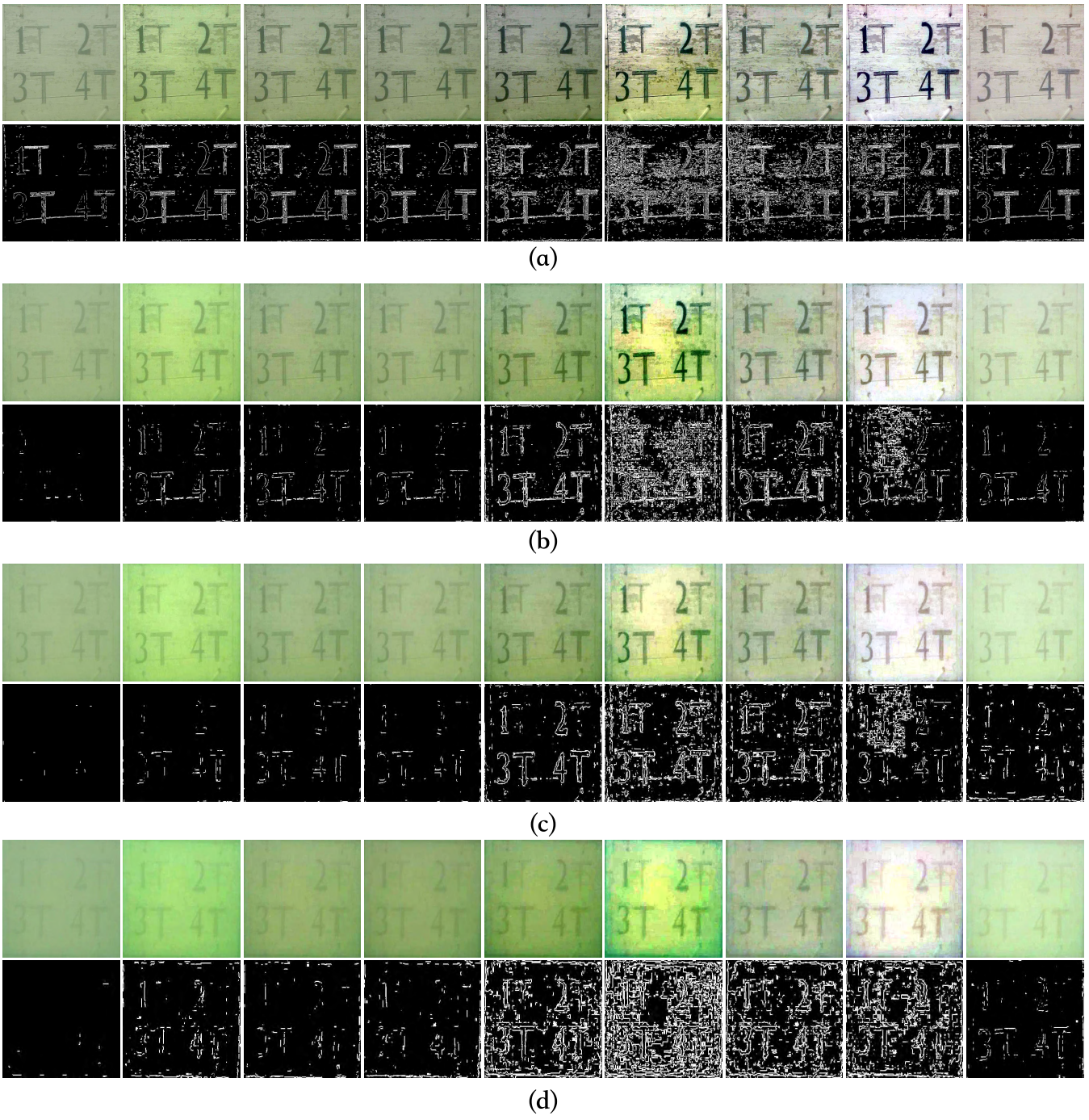

FIGURE 8. Cropped images of the calibration board and edge map. From right to left: original images and edges, DCP results and edges, CAP results and edges, DehazeNet results and edges, MSCNN results and edges, NON results and edges, CLAHE results and edges, Retinex results and edges, and MAI results and edges.

meaningful information or only the noise point is difficult. Thus, in this experiment, we only evaluate the calibration board area while ignoring the background area. The calibration board area is carefully cropped from the processed images and resized to the same size. Then, the edge and gradient coefficients are computed using Eqs. 13 and 14. Fig. 8 shows the cropped areas and the corresponding edges. The edges are detected as larger than 5% of the change in the entire gradient.

Tables 1 and 2 show the n_e and r_e coefficients of different distances for different methods. We observe that, when the object board is near the camera (120 *mm*), the visibility is good. Thus, the contrast ratios n_e and r_e of all of the methods are only moderately enhanced. When

TABLE 1. Comparison of the visibility recovery coefficient n_e of four images.

distance (mm)	DCP	CAP	DehazeNet	MSCNN	NON	CLAHE	Retinex	MAI
120	1.1051	1.1247	1.1369	2.6609	5.6529	5.0067	3.3684	1.2305
210	8.2843	8.0561	5.5203	28.559	88.2727	39.3133	39.2863	6.7176
270	9.3435	13.1465	10.8599	51.9682	124.8408	88.6369	84.5541	12.0637
360	13.6161	16.433	12.8795	58.1499	108.1563	60.3884	64.5134	13.8616

TABLE 2. Comparison of the visibility recovery coefficient r_e of four images.

distance (mm)	DCP	CAP	DehazeNet	MSCNN	NON	CLAHE	Retinex	MAI
120	0.7792	0.8147	0.7457	0.9977	1.0716	1.0482	0.9876	0.9417
210	0.9495	0.8901	0.8625	0.9874	1.005	1.0095	0.986	0.9699
270	0.9619	0.9592	0.9443	0.9984	1.0107	1.0057	0.9982	0.9757
360	0.9808	1.0044	0.9822	1.0096	1.0121	1.0174	1.0043	1.0012

the distance of the object board to the camera increases (210, 270, and 360 mm), the visibility of the original images is decreased and the contrast ratios n_e and r_e of all of the methods are significantly enhanced. In general, MSCNN, NON, CLAHE, and Retinex exhibit high contrast enhancement, whereas DCP, CAP, and DehazeNet exhibit low contrast enhancement. Compared with that shown in Fig. 8, the edge results of DCP, CAP, and DehazeNet are unclear. Those of MSCNN, NON, CLAHE, and Retinex introduce fake edge points, such as the amplified illumination distortion. The resulting edge map of MAI detects true edges clearly and eliminates illumination distortion correctly. Notably, it is true that the proposed method does not perform largest or weakest in every norm. We believe that the criterion of a successful restoration method is the best overall performance. For example, the contrast amplification should be moderate, for a small one may be not enough and a too large one may cause distortion. So combined with the visual performance shown in Fig. 8, MAI works in an appropriate way.

2) COLOR CORRECTION

In the previous section, we compare the contrast enhancement of different restoration methods. In this section, we examine another important characteristic of image restoration, that is, color correction. For this end, we consider the atmosphere image of the colormap board taken by the same camera with the underwater images as the ground truth image (as shown in Fig. 9). Then, we compute the mean square error (MSE) for each raw and restored image. The MSE measures the difference of two images. A low MSE indicates that the two compared images are similar to each other, and vice versa. We should achieve a low MSE for underwater image restoration to obtain a good color correction performance. We also manually crop the colormap board area carefully from each processed image to eliminate the effect of the background when calculating the MSE.

FIGURE 9. Ground truth colormap board image.

Fig. 10 shows the cropped areas of the raw images and the results of the different algorithms. The corresponding MSE for each image is plotted in Fig. 11 to show the tendency of change directly. Clearly, except for Retinex, the MSE for the other methods all increases with the increase in the camera distance. MSCNN, DehazeNet, CAP, NON, and DCP obtain higher MSE than that of original images, indicating that they introduce severe color distortion. For each fixed distance, our algorithm exhibits the lowest MSE. Notably, the MSE of Retinex decreases with the increase in the camera distance. This phenomenon is irrational. However, carefully examining the resulting image reveals the reason. Retinex may lead to bias on the entire colormap in the form of changes to the mean value rather than different effects on different colors. Thus, the contrast decreases with the increase in the distance. The bias also decreases, which results in a low MSE. Although Retinex obtains a lower MSE than that of our MAI at a distance of 360 mm, we still assert that our algorithm can obtain a better color correction effect.

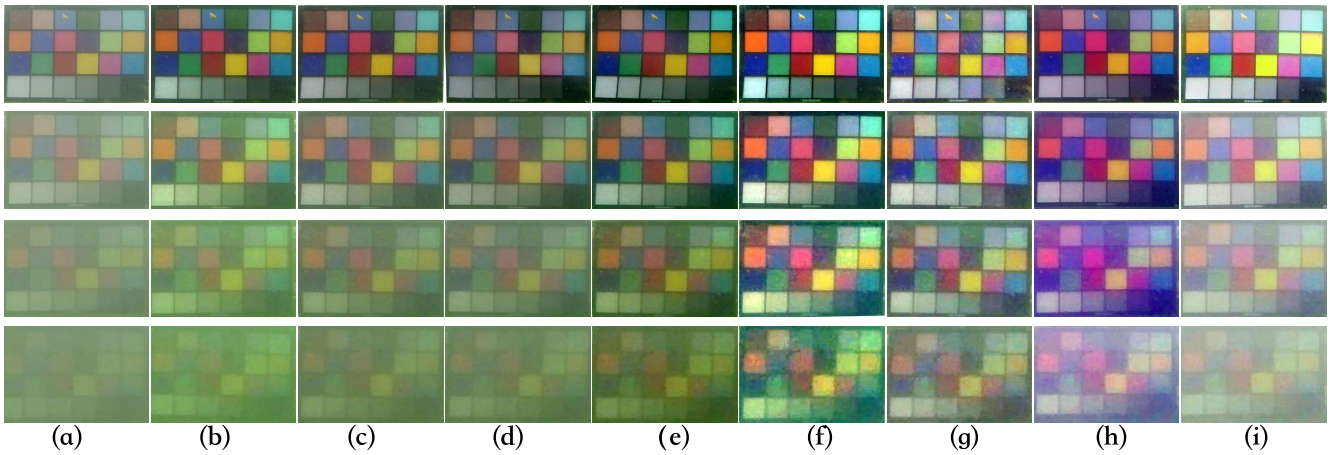

FIGURE 10. (a) Raw images of the colormap board: from top to bottom, the distances from the camera to the object are 120, 210, 270, and 360 *mm*; (b) results of DCP; (c) results of CAP; (d) results of DehazeNet; (e) results of MSCNN; (f) results of NON; (g) results of CLAHE; (h) results of Retinex; and (i) results of MAI.

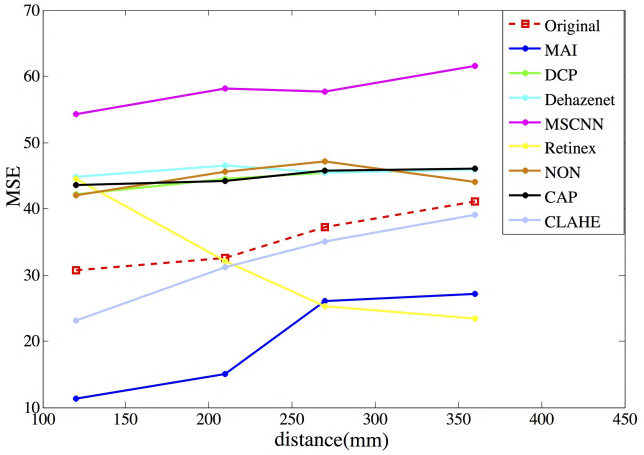

FIGURE 11. MSE curve for the different methods.

VI. CONCLUSION AND DISCUSSION

In this study, we propose an image restoration method, which aims at enhancing the contrast and correcting the color distortion of underwater images. The proposed MAI-based algorithm considers not only the scattering but also the attenuation as a whole as the transmission coefficient. First, we use the maximum map of the red channel to derive the depth map, slice the entire image to small pieces, and estimate the background light for each piece. The overall background light is obtained by linear interpolation to the background pieces. Second, based on the simplified light propagation model, the transmission map is estimated for the *R*, *G*, and *B* colors separately. Three groups of images are taken as our experimental images: one is natural underwater scene and the two other are images of a calibration board coupled with a color RGB tank and a colormap board. The subjective and objective tests show that the proposed method performs well in terms of contrast enhancement and color correction.

However, given that we use certain prior knowledge, that is, the red channel light attenuates fastest, to derive the depth map, the assumption may not adapt to several special conditions. For example, when the real large-scale object is nearly dark, such as a diver who wears a black diving suit, the prior knowledge may be inappropriate and the processing result may appear distorted. For most instances, the underwater world is colorful. Thus, the proposed method can work well most of the time.

REFERENCES

[1] S. Q. Duntley, "Light in the sea," *J. Opt. Soc. Amer.*, vol. 53, no. 2, pp. 214–233, 1963.
[2] R. Schettini and S. Corchs, "Underwater image processing: State of the art of restoration and image enhancement methods," *EURASIP J. Adv. Signal Process.*, vol. 2010, no. 1, p. 746052, 2010
[3] J. S. Jaffe, "Underwater optical imaging: The past, the present, and the prospects," *IEEE J. Ocean. Eng.*, vol. 40, no. 3, pp. 683–700, Jul. 2015.
[4] J. S. Jaffe, K. D. Moore, J. McLean, and M. P. Strand, "Underwater optical imaging: Status and prospects," *Oceanography*, vol. 14, no. 3, pp. 66–76, 2001.
[5] G. R. Fournier, D. Bonnier, J. L. Forand, and P. W. Pace, "Range-gated underwater laser imaging system," *Opt. Eng.*, vol. 32, no. 9, pp. 2185–2190, 1993.
[6] S. G. Demos and R. R. Alfano, "Optical polarization imaging," *Appl. Opt.*, vol. 36, no. 1, pp. 150–155, 1997.
[7] Y. Gu *et al.*, "Polarimetric imaging and retrieval of target polarization characteristics in underwater environment," *Appl. Opt.*, vol. 55, no. 3, pp. 626–637, 2016.
[8] H. Lu, Y. Li, Y. Zhang, M. Chen, S. Serikawa, and H. Kim, "Underwater optical image processing: A comprehensive review," *Mobile Netw. Appl.*, vol. 2010, pp. 1–8, Apr. 2017.
[9] B. L. McGlamery, "A computer model for underwater camera systems," *Ocean Opt.*, vol. 208, pp. 221–231, Jan. 1979.
[10] W. Hou, D. J. Gray, A. D. Weidemann, and R. A. Arnone, "Comparison and validation of point spread models for imaging in natural waters," *Opt. Exp.*, vol. 16, no. 13, pp. 9958–9965, 2008.
[11] E. Trucco and A. T. Olmos-Antillon, "Self-tuning underwater image restoration," *IEEE J. Ocean. Eng.*, vol. 31, no. 2, pp. 511–519, Apr. 2006.
[12] Z. Liu, Y. Yu, K. Zhang, and H. Huang, "Underwater image transmission and blurred image restoration," *Opt. Eng.*, vol. 40, no. 6, pp. 1125–1131, 2001.
[13] G. Wang, B. Zheng, and F. F. Sun, "Estimation-based approach for underwater image restoration," *Opt. Lett.*, vol. 36, no. 13, pp. 2384–2386, 2011.

[14] H. Lu, Y. Li, S. Nakashima, H. Kim, and S. Serikawa, "Underwater image super-resolution by descattering and fusion," *IEEE Access*, vol. 5, pp. 670–679, 2017.
[15] K. Zuiderveld, "Contrast limited adaptive histogram equalization," *Graph. Gems*, vol. 11, pp. 474–485, Jan. 1994.
[16] J.-M. Morel, A. B. Petro, and C. Sbert, "Fast implementation of color constancy algorithms," *Proc. SPIE*, vol. 7241, p. 724106, 2009.
[17] C. Ancuti, C. O. Ancuti, T. Haber, and P. Bekaert, "Enhancing underwater images and videos by fusion," in *Proc. IEEE Conf. Comput. Vis. Pattern Recognit.*, Jun. 2012, pp. 81–88.
[18] A. S. A. Ghani and N. A. M. Isa, "Underwater image quality enhancement through composition of dual-intensity images and Rayleigh-stretching," *SpringerPlus*, vol. 3, p. 757, Dec. 2014.
[19] A. S. A. Ghani and N. A. M. Isa, "Enhancement of low quality underwater image through integrated global and local contrast correction," *Appl. Soft Comput.*, vol. 37, pp. 332–344, Dec. 2015.
[20] A. S. A. Ghani and N. A. M. Isa, "Underwater image quality enhancement through integrated color model with Rayleigh distribution," *Appl. Soft Comput.*, vol. 27, pp. 219–230, Feb. 2015.
[21] J. Han *et al.*, "Resolution enhancement in active underwater polarization imaging with modulation transfer function analysis," *Appl. Opt.*, vol. 54, no. 11, pp. 3294–3302, 2015.
[22] H. Lu *et al.*, "Underwater image enhancement method using weighted guided trigonometric filtering and artificial light correction," *J. Vis. Commun. Image Represent.*, vol. 38, pp. 504–516, Jul. 2016.
[23] D. Berman, T. Treibitz, and S. Avidan, "Non-local image dehazing," in *Proc. IEEE Conf. Comput. Vis. Pattern Recognit.*, Jun. 2016, pp. 1674–1682.
[24] B. Cai, X. Xu, K. Jia, C. Qing, and D. Tao, "DehazeNet: An end-to-end system for single image haze removal," *IEEE Trans. Image Process.*, vol. 25, no. 11, pp. 5187–5198, Nov. 2016.
[25] W. Ren, S. Liu, H. Zhang, J. Pan, X. Cao, and M. H. Yang, "Single image dehazing via multi-scale convolutional neural networks," in *Proc. Eur. Conf. Comput. Vis.*, Oct. 2016, pp. 154–169.
[26] Y. Li, R. T. Tan, and M. S. Brown, "Nighttime haze removal with glow and multiple light colors," in *Proc. IEEE Conf. Comput. Vis. Pattern Recognit.*, Dec. 2015, pp. 226–234.
[27] Q. Zhu, J. Mai, and L. Shao, "A fast single image haze removal algorithm using color attenuation prior," *IEEE Trans. Image Process.*, vol. 24, no. 11, pp. 3522–3533, Nov. 2015.
[28] I. Riaz, T. Yu, Y. Rehman, and H. Shin, "Single image dehazing via reliability guided fusion," *J. Vis. Commun. Image Represent.*, vol. 40, pp. 85–97, Oct. 2016.
[29] K. He, J. Sun, and X. Tang, "Single image haze removal using dark channel prior," *IEEE Trans. Pattern Anal. Mach. Intell.*, vol. 33, no. 12, pp. 2341–2353, Dec. 2011.
[30] N. Carlevaris-Bianco, A. Mohan, and R. M. Eustice, "Initial results in underwater single image dehazing," in *Proc. OCEANS MTS/IEEE Seattle*, Sep. 2010, pp. 1–8.
[31] J. Y. Chiang and Y.-C. Chen, "Underwater image enhancement by wavelength compensation and dehazing," *IEEE Trans. Image Process.*, vol. 21, no. 4, pp. 1756–1769, Apr. 2012.
[32] A. Galdran, D. Pardo, A. Picón, and A. Alvarez-Gila, "Automatic red-channel underwater image restoration," *J. Vis. Commun. Image Represent.*, vol. 26, pp. 132–145, Jan. 2015.
[33] C. Li, J. Quo, Y. Pang, S. Chen, and J. Wang, "Single underwater image restoration by blue-green channels dehazing and red channel correction," in *Proc. IEEE Int. Conf. Acoust., Speech Signal Process.*, Mar. 2016, pp. 1731–1735.
[34] N. Hautière, J.-P. Tarel, D. Aubert, and É. Dumont, "Blind contrast enhancement assessment by gradient ratioing at visible edges," *Image Anal. Stereol. J.*, vol. 27, no. 2, pp. 87–95, Jun. 2008.

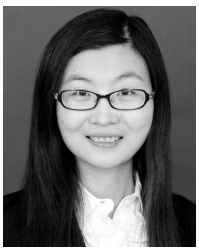

NAN WANG (M'16) received the B.S. degree in measurement and control technology and instrument and the M.S. and Ph.D. degrees in instrument science and technology from Southeast University, Nanjing, China, in 2009, 2012, and 2015, respectively.

In 2016, she joined the Department of Electronic Engineering, Ocean University of China, where, she is currently a Lecturer. Her research interests include underwater image processing, logical stochastic resonance, and robotics.

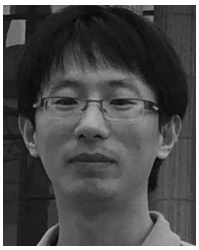

HAIYONG ZHENG (M'12) received the B.S. degree in electronic information engineering and the Ph.D. degree in ocean information sensing and processing from the Ocean University of China, Qingdao, China, in 2004 and 2009, respectively.

In 2009, he joined the Department of Electronic Engineering, Ocean University of China, where he is currently an Associate Professor. His research interests include image processing, computer vision, and machine learning.

BING ZHENG (M'07) received the B.S. degree in electronics and information system, the M.S. degree in marine physics, and the Ph.D. degree in computer application technology from the Ocean University of China, Qingdao, China, in 1991, 1995, and 2013, respectively.

He is currently a Professor with the Department of Electronic Engineering, Ocean University of China. His research interests include ocean optics, underwater imaging, and optical detection.